Spin-orbit coupling and Kondo resonance in the Co adatom on the Cu(100) surface: DFT plus exact diagonalization study

A. B. Shick* and M. Tchaplianka
Institute of Physics, Czech Academy of Science, Na Slovance 2, CZ-18221 Prague, Czech Republic

A. I. Lichtenstein
Institute of Theoretical Physics, University of Hamburg, D-20355 Hamburg, Germany
and European X-Ray Free-Electron Laser Facility, Holzkoppel 4, D-22869 Schenefeld, Germany

(Received 26 May 2022; revised 11 October 2022; accepted 29 November 2022; published 12 December 2022)

We report density functional theory plus exact diagonalization of the multiorbital Anderson impurity model calculations for the Co adatom on the top of a Cu(001) surface. For the Co atom d-shell occupation $n_d \approx 8$, a singlet many-body ground state and Kondo resonance are found, when the spin-orbit coupling is included in the calculations. The differential conductance is evaluated in good agreement with the scanning tunneling microscopy measurements. The results illustrate the essential role which the spin-orbit coupling is playing in the formation of a Kondo singlet for the multiorbital impurity in low dimensions.

DOI: 10.1103/PhysRevB.106.245115

I. INTRODUCTION

Electronic nanometer-scaled devices require the atomistic control of their behavior governed by electron correlation effects. One of the most famous correlation phenomena is the Kondo effect originating from screening of a local magnetic moment by a Fermi sea of conduction electrons, and resulting in the formation of a singlet ground state [1]. Historically, Kondo screening was detected as a resistance increase below a characteristic Kondo temperature T_K in dilute magnetic alloys [2]. Recent advances in scanning tunneling microscopy (STM) allowed the observation of the Kondo phenomenon on the atomic scale, for atoms and molecules at the surfaces [3,4]. In these experiments, an enhanced conductance near the Fermi level (E_F) is found due to the formation of a sharp Abrikosov-Suhl-Kondo [5–7] resonance in the electronic density of states (DOS).

One of the most experimentally and theoretically studied cases of the Kondo effect is that of a Co adatom on a metallic Cu substrate [3,8–10]. The experimental STM spectra display sharp peaks at zero bias, or so-called "zero-bias" anomalies, similar to the Fano resonance [11] found in atomic physics, which are associated with Kondo resonance. A theoretical description of the Kondo screening in multiorbital d manifolds is difficult since the whole d shell is likely to play a role. Very recently, a theoretical electronic structure of a Co atom on the top of Cu(100) was considered [10] using the numerically exact continuous-time quantum Monte Carlo (CTQMC) method [12] to solve the multiorbital single impurity Anderson model [13] (SIAM) together with the density functional theory [14] as implemented in the W2DYNAMICS package [15,16]. However, the spin-orbit coupling (SOC) was neglected. The peak in the DOS at E_F was obtained in these calculations, and was interpreted as a signature of Kondo resonance.

An alternative interpretation was proposed [17] which is based on the spin-polarized time-dependent DFT in conjunction with many-body perturbation theory. These authors claim that the "zero-bias" anomalies are not necessarily related to Kondo resonance, and are connected to the interplay between inelastic spin excitations and magnetic anisotropy. Thus a controversy exists concerning the details of the physical processes underlying the Kondo screening in Co@Cu(100). In this paper, we revisit the Co@Cu(100) case making use of the combination of DFT with the exact diagonalization of multiorbital SIAM (DFT+ED) including SOC. We demonstrate that SOC plays a crucial role in the formation of a singlet ground state (GS) and Kondo resonance.

II. METHODOLOGY: DFT+EXACT DIAGONALIZATION

The exact diagonalization (ED) method is based on a numerical solution of the multiorbital Anderson impurity model (AIM) [13]. The continuum of the bath states is discretized. The five d-orbital AIM with a full spherically symmetric Coulomb interaction, a crystal field (CF), and SOC is written as

$$\begin{aligned} H = &\sum_{km\sigma} \epsilon_{km} b^\dagger_{km\sigma} b_{km\sigma} + \sum_{m\sigma} \epsilon_d d^\dagger_{m\sigma} d_{m\sigma} \\ &+ \sum_{mm'\sigma\sigma'} (\xi \mathbf{l}\cdot\mathbf{s} + \mathbf{\Delta_{CF}})^{\sigma\ \sigma'}_{mm'} d^\dagger_{m\sigma} d_{m'\sigma'} \\ &+ \sum_{km\sigma} (V_{km} d^\dagger_{m\sigma} b_{km\sigma} + \text{H.c.}) \\ &+ \frac{1}{2} \sum_{mm'm''m'''\sigma\sigma'} U_{mm'm''m'''} d^\dagger_{m\sigma} d^\dagger_{m'\sigma'} d_{m'''\sigma'} d_{m''\sigma}. \end{aligned} \quad (1)$$

*shick@fzu.cz

The impurity-level position ϵ_d which yields the desired $\langle n_d \rangle$, and the bath energies ϵ_{km} are measured from the chemical potential μ, that was set to zero. The SOC ξ parameter specifies the strength of the spin-orbit coupling, whereas the $\Delta_{\rm CF}$ matrix describes the CF acting on the impurity. The hybridization V_{mk} parameters describe the coupling of the substrate to the impurity orbitals. These parameters are determined from DFT calculations, and their particular choice will be described below.

The last term in Eq. (1) represents the Coulomb interaction. The Slater integrals $F_0 = 4.00$ eV, $F_2 = 7.75$ eV, and $F_4 = 4.85$ eV are used for the Coulomb interaction [9,10]. They correspond to the values for the Coulomb $U = 4$ eV and exchange $J = 0.9$ eV for Co which are in the ballpark of commonly accepted U and J for transitional $3d$ metals.

The DFT calculations were performed on a supercell of four Cu(100) layers, and the Co adatom followed by four empty Cu layers modeling the vacuum. Figure 1(a) shows the ball model of the Co@[$4Cu_8$] supercell employed for the adsorbate atop of Cu. The structure relaxation was performed employing the VASP method [18] together with the generalized gradient approximation (GGA) to spin-polarized DFT without SOC. The adatom-substrate distance as well as the atomic positions within two Cu(100) layers underneath were allowed to relax. The relaxed distance between the Co adatom in a fourfold hollow position and the first Cu substrate layer of 2.91 a.u. is in good agreement with the previously reported value of 2.87 a.u. [10].

In order to obtain the bath parameters in the AIM Hamiltonian Eq. (1), we make use of the recipes of the dynamical mean-field theory (DMFT) [19,20], and employ the DFT [local density approximation (LDA)] local Green's function $G_0(z)$,

$$[G_0(z)]_{\gamma_1\gamma_2} = \frac{1}{V_{\rm BZ}} \int_{\rm BZ} d^3k [z + E_F - H_{\rm DFT}(\mathbf{k})]^{-1}_{\gamma_1\gamma_2}, \qquad (2)$$

calculated with the help of the full-potential linearized augmented plane-wave method (FLAPW) [21,22], in order to define the parameters for Eq. (1). Here, the energy z is counted from the Fermi energy E_F, and the index $\gamma \equiv lm\sigma$ marks the d orbitals in the muffin-tin (MT) sphere of the Co adatom. Note that the non-spin-polarized LDA is used to extract the hybridization function $\Delta(z)$. The orbitally resolved density of states (DOS) together with the hybridization function Im Δ are shown in Figs. 1(b) and 1(c). They are compatible with the results of Ref. [23]. Further details of constructing the discrete bath model are given in Appendix A.

The SOC parameter $\xi = 0.079$ eV is taken from LDA calculations in a standard way,

$$\xi = \int_0^{R_{\rm MT}} dr r \frac{1}{2(Mc)^2} \frac{dV(r)}{dr} [u_l(r)]^2,$$

making use of the radial solutions u_l of the Kohn-Sham-Dirac scalar-relativistic equations [24], the relativistic mass $M = m + (E_l - V(r))/2c^2$ at an appropriate energy E_l, and the radial derivative of the spherically symmetric part of the LDA potential.

III. RESULTS AND DISCUSSION

The total number of electrons N, and the d-shell occupation are controlled by the ϵ_d parameter. It has a meaning of the chemical potential $\mu = -\epsilon_d$ in Eq. (1). In DMFT it is quite common to use $\mu = V_{\rm dc}$, the spherically symmetric double counting which has a meaning of the mean-field Coulomb energy of the d shell, and to use standard [around mean-field (AMF)] $V_{\rm dc} = (U/2\, n_d + \frac{2l}{2(2l+1)}(U - J)n_d)$ [25] form, or the fully localized limit (FLL) $V_{\rm dc} = (U - J)/2\ (n_d - 1)$ [26]. Since the precise definition of n_d depends on the choice of localized basis, we adopt the strategy of Ref. [9], and consider a value of μ as a parameter.

A. Co in bulk Cu

At first, we consider the Co impurity in bulk Cu making use of the $CoCu_{15}$ supercell model. DFT+ED calculations for different values of μ in comparison with previous DFT+CTQMC results [9] are described in detail in Ref. [27]. Here, we adjust the value of μ in order to have the Co atom d-shell occupation $n_d \approx 8$. This valence of Co in bulk Co follows from DFT calculations [9,27].

Without SOC we found that the value of $\mu = 27.4$ corresponds to $n_d \approx 8$ occupation. The GS solution without SOC (see Table I) is the $|\Omega\rangle_{N=30}$ singlet, and the excited triplet is ≈0.4 eV higher in the energy. Note that each eigenstate $|\Omega\rangle_N$ of Eq. (1) corresponds to an integer N occupation (d shell+bath) since $\hat{N}$ commutes with Hamiltonian Eq. (1). For each $|\Omega\rangle$, the probabilities of finding the atomic eigenstates $|n\rangle$ with integer occupation d^n, $P_n = \langle n|\Omega\rangle\langle\Omega|n\rangle$, and the d-shell occupation $n_d = \sum_n P_n n_{d^n}$.

The corresponding density of d states (DOS) [1],

$$A(\epsilon) = -\frac{1}{\pi Z} {\rm Im} \sum_{\gamma,\alpha,\beta} \frac{\langle\Omega_\alpha|c_\gamma|\Omega_\beta\rangle\langle\Omega_\beta|c^\dagger_\gamma|\Omega_\alpha\rangle}{\epsilon + i\delta + E_\alpha - E_\beta} \times [e^{-\beta E_\beta} + e^{-\beta E_\alpha}], \qquad (3)$$

where α, β run over the eigenstates of Hamiltonian Eq. (1), and $\gamma \equiv \{m, \sigma\}$ marks the single-particle spin orbital, is shown in Fig. 2(a), with the peak in DOS very near E_F.

The expectation values of the total $\langle\Omega|J_z|\Omega\rangle$, orbital $\langle\Omega|L_z|\Omega\rangle$, and spin $\langle\Omega|S_z|\Omega\rangle$ $3d$-shell projected angular momenta for the $|\Omega\rangle_{N=30}$ singlet GS and the excited triplet are shown in Table I. They correspond to a solution of the Kondo model for localized $S = \frac{1}{2}$ antiferromagnetically coupled to a single band of conduction electrons [28]. Together with the Kondo peak in DOS [cf. Fig. 2(a)] our DFT+ED solution corresponds to the Kondo singlet state.

When SOC is included, and the spin is not a good quantum number, there are minor changes in the character for $\mu = 27.5$ ($n_d \approx 8$), the GS solution $|\Omega\rangle_{N=30}$: GS is a singlet, and the excited triplet consists of effective $|J = 1, J_z = -1, 0, 1\rangle$ degenerate states which are ≈0.5 eV higher in energy. The DOS has a peak in DOS very near E_F. It is seen that weak $3d$-shell SOC plays no essential role for the Co impurity in the Cu host. These calculations show that our DFT+ED approach is capable of reproducing the Kondo singlet for Co in bulk Cu for $n_d = 8$, in agreement with the conclusions of DFT+CTQMC [9]. Also, in agreement with the commonly accepted point of

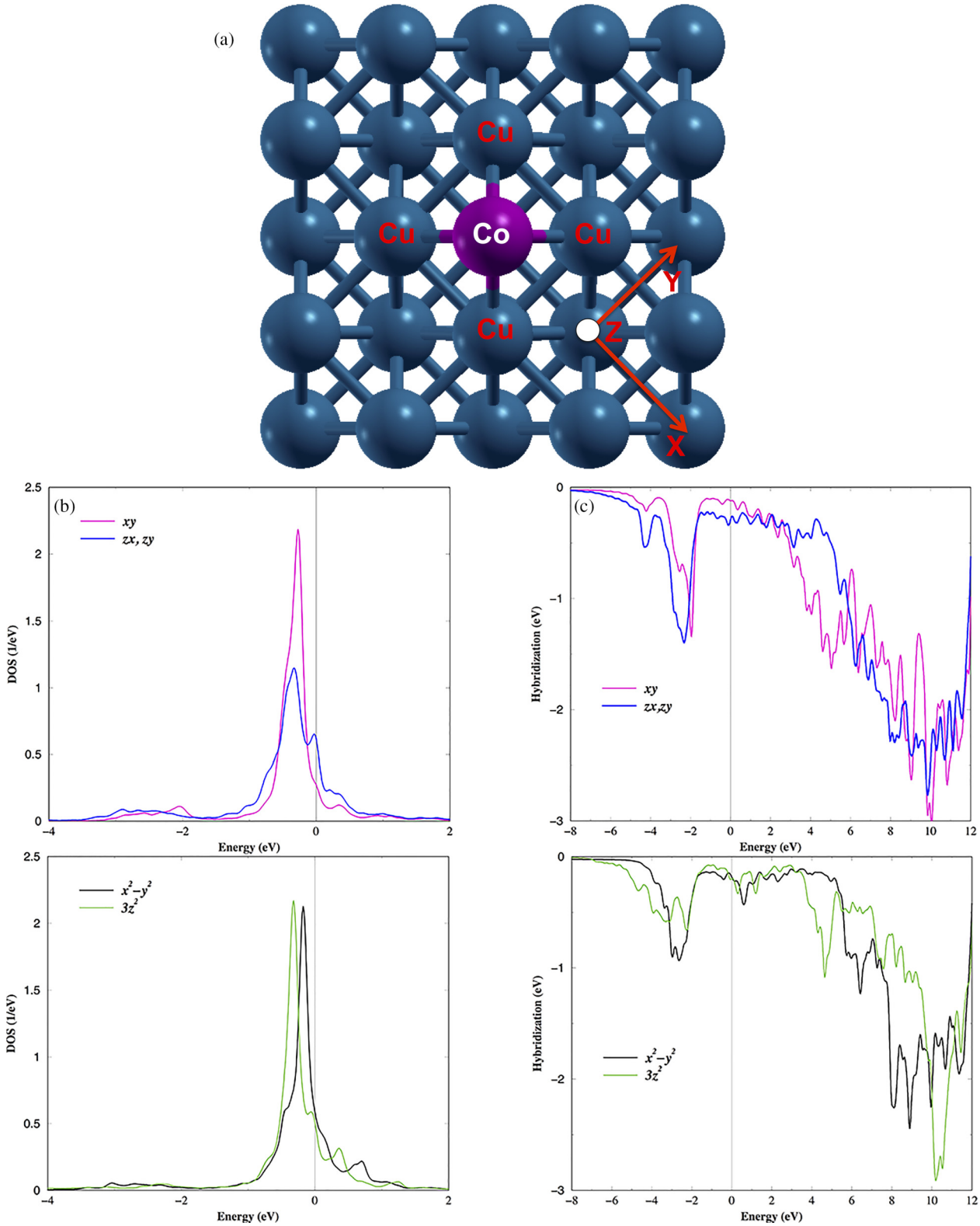

FIG. 1. (a) The ball model (top view) for a Co@[$4Cu_8$] supercell. The specific choice of Cartesian reference frame is show. With this choice, the local Green's function without SOC becomes diagonal in the basis of cubic harmonics $m = \{xz, yz, xy, x^2 - y^2, 3z^2 - r^2\}$. (b) Orbitally resolved DOS. (c) Orbitally resolved hybridization Im Δ for a Co adatom on Cu(001).

view [29], we show that the presence of SOC does not lead to an essential modification of a Kondo model.

B. Co on Cu(001)

Now we turn to a salient aspect of our investigation, the Co adatom on a Cu(001) surface. Considering a value of μ

TABLE I. The total number of particles (d shell+bath) N, the expectation values $\langle\Omega|J_z|\Omega\rangle$, $\langle\Omega|L_z|\Omega\rangle$, and $\langle\Omega|S_z|\Omega\rangle$ of $3d$-shell projected angular momenta, nonzero probabilities P_{d^n} to find the atomic eigenstates $|n\rangle$ with integer occupation d^n for GS, and low-energy excitation energies for different values of μ.

	Energy (eV)	J_z	L_z	S_z	P_{d^7}	P_{d^8}	P_{d^9}
			Without SOC				
		$\mu = 27.4$ eV, $n_d = 8.05$					
N=30	−148.5822	0.	0.	0.	0.20	0.51	0.26
	−148.1014	0.53	0	0.53	0.22	0.55	0.20
	−148.1014	0	0	0	0.22	0.55	0.20
	−148.1014	−0.53	0	−0.53	0.22	0.55	0.20
			With SOC				
	Energy (eV)	J_z	L_z	S_z	P_{d^7}	P_{d^8}	P_{d^9}
		$\mu = 27.5$ eV, $n_d = 7.99$					
N=30	−149.4028	0.	0.	0.	0.19	0.51	0.27
	−148.9296	0.94	0.49	0.45	0.21	0.55	0.21
	−148.9296	0.	0.	0.	0.21	0.55	0.21
	−148.9296	−0.94	−0.49	−0.45	0.21	0.55	0.21

as a parameter, we analyze the ground state (GS) of Eq. (1) with and without SOC for different values of μ. Making use of grand-canonical averages at low temperature $k_BT = \beta^{-1} = (1/500)$ eV (20 K) we calculate the expectation values of the total number of electrons (d shell+bath) $\langle N\rangle$, the charge fluctuation $(\langle N^2\rangle - \langle N\rangle^2)^{\frac{1}{2}}$ near the GS, and the expectation values of spin (S), orbital (L), and total spin-orbital (J) $3d$-shell moments, and show them in Table II together with the d-shell occupation n_d for the GS, and the corresponding P_n probabilities, with and without SOC.

For the values of $\mu = 26$ and 27 eV, the GS is the eigenstate $|\Omega\rangle_{N=26}$, and is a combination of d^7 ($P_{d^7} \approx 0.3$) and d^8 ($P_{d^8} \approx 0.6$). These states have a noninteger n_d occupation due to the hybridization of the atomic d states with the substrate. Nevertheless, $(\langle N^2\rangle - \langle N\rangle^2)^{\frac{1}{2}} \approx 0$, pointing to the absence of charge fluctuations. The S values lie between $S = 3/2$ (the atomic d^7, ^4F), and $S = 1$ (the atomic d^8, ^3F), while L is close to the atomic $L = 3$. The expectation values of the z-axis projections of the total $\langle\Omega|J_z|\Omega\rangle$, orbital $\langle\Omega|L_z|\Omega\rangle$, and spin $\langle\Omega|S_z|\Omega\rangle 3d$-shell angular momenta for GS and low-energy excitation energies for $\mu = 27.0$ eV are shown in Table III. It is seen that without SOC the GS can be interpreted as an $S =$ 1-like triplet. For $\mu = 28$ eV, the GS is the eigenstate $|\Omega\rangle_{N=27}$, and the contributions of d^7 ($P_{d^7} \approx 0.1$) and d^8 ($P_{d^8} \approx 0.5$) are

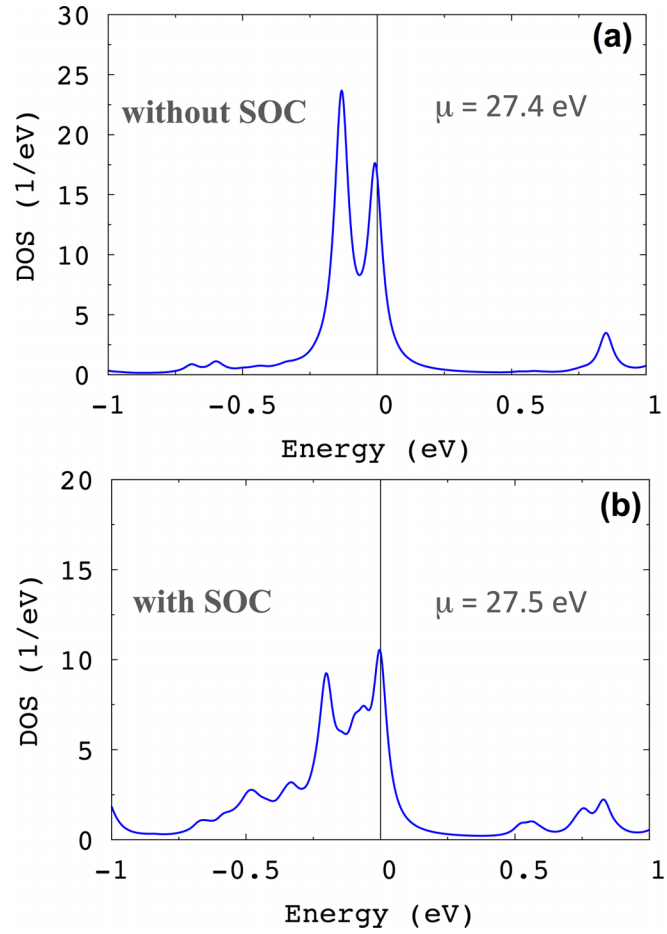

FIG. 2. (a) DOS for Co in bulk Cu without SOC for $\mu = 27.4$ eV, and (b) with SOC for $\mu = 27.5$ eV.

TABLE II. The chemical potential μ (eV), the occupation $\langle N\rangle$, fluctuation $(\langle N^2\rangle - \langle N\rangle^2)^{\frac{1}{2}}$, n_d occupation, nonzero probabilities P_{d^n} to find the atomic eigenstates $|n\rangle$ with integer occupation d^n, and spin, orbital, and total moments of the impurity d shell for different values of μ. Grand-canonical averages are at low temperature $k_BT = \beta^{-1} = (1/500)$ eV.

μ (eV)	$\langle N\rangle$	$(\langle N^2\rangle - \langle N\rangle^2)^{\frac{1}{2}}$	n_d	P_{d^6}	P_{d^7}	P_{d^8}	P_{d^9}	S	L	J
					Without SOC					
26	26.00	0.00	7.57	0.05	0.34	0.56	0.03	1.10	3.07	3.40
27	26.00	0.01	7.74	0.03	0.27	0.62	0.08	1.03	3.01	3.32
27.4	26.55	0.50	7.93	0.02	0.21	0.58	0.18	0.94	2.87	3.15
28	27.00	0.00	8.17	0.01	0.14	0.51	0.33	0.82	2.68	2.91
					With SOC					
μ (eV)	$\langle N\rangle$	$(\langle N^2\rangle - \langle N\rangle^2)^{\frac{1}{2}}$	n_d	P_{d^6}	P_{d^7}	P_{d^8}	P_{d^9}	S	L	J
26	26.00	0.00	7.58	0.05	0.34	0.57	0.04	1.09	3.07	3.89
27	26.00	0.00	7.75	0.03	0.26	0.62	0.08	1.03	3.01	3.82
27.6	26.38	0.48	7.96	0.02	0.20	0.58	0.19	0.93	2.86	3.51
28	27.00	0.00	8.17	0.01	0.14	0.51	0.33	0.82	2.68	3.16

TABLE III. The total number of particles (d shell+bath) N, the expectation values $\langle\Omega|J_z|\Omega\rangle$, $\langle\Omega|L_z|\Omega\rangle$, and $\langle\Omega|S_z|\Omega\rangle$ of $3d$-shell projected angular momenta, nonzero probabilities P_{d^n} to find the atomic eigenstates $|n\rangle$ with integer occupation d^n for GS, and low-energy excitation energies for different values of μ.

			Without SOC				
	Energy (eV)	J_z	L_z	S_z	P_{d^7}	P_{d^8}	P_{d^9}
			$\mu = 27.0$ eV				
$N = 26$	−142.2319	0.0	0.0	0.0	0.27	0.62	0.08
	−142.2319	0.90	0.0	0.90	0.27	0.62	0.08
	−142.2319	−0.90	0.0	−0.90	0.27	0.62	0.08
			$\mu = 27.4$ eV				
$N = 26$	−145.3478	0.00	0.0	0.00	0.23	0.61	0.13
	−145.3478	0.81	0.0	0.81	0.23	0.61	0.13
	−145.3478	−0.81	0.0	−0.81	0.23	0.61	0.13
$N = 27$	−145.3490	0.57	0.0	0.57	0.19	0.55	0.23
	−145.3490	−0.57	0.0	−0.57	0.19	0.55	0.23
			$\mu = 28.0$ eV				
$N = 27$	−150.1992	0.53	0.0	0.53	0.14	0.51	0.33
	−150.1992	−0.53	0.0	−0.53	0.14	0.51	0.33
			With SOC				
	Energy (eV)	J_z	L_z	S_z	P_{d^7}	P_{d^8}	P_{d^9}
			$\mu = 27.0$ eV				
$N = 26$	−142.3054	0.00	0.0	0.00	0.26	0.62	0.08
	−142.3009	1.48	0.91	0.57	0.26	0.62	0.08
	−142.3009	−1.48	−0.91	−0.57	0.26	0.62	0.08
			$\mu = 27.6$ eV				
$N = 26$	−146.9950	0.00	0.0	0.00	0.21	0.61	0.16
	−146.9912	1.10	0.70	0.40	0.21	0.61	0.16
	−146.9912	−1.10	−0.70	−0.40	0.21	0.61	0.16
N=27	−146.9931	1.43	0.95	0.48	0.18	0.54	0.26
	−146.9931	−1.43	−0.95	−0.48	0.18	0.54	0.26
			$\mu = 28.0$ eV				
N=27	−150.2373	1.37	0.91	0.45	0.14	0.51	0.33
	−150.2373	−1.37	−0.91	−0.45	0.14	0.51	0.33

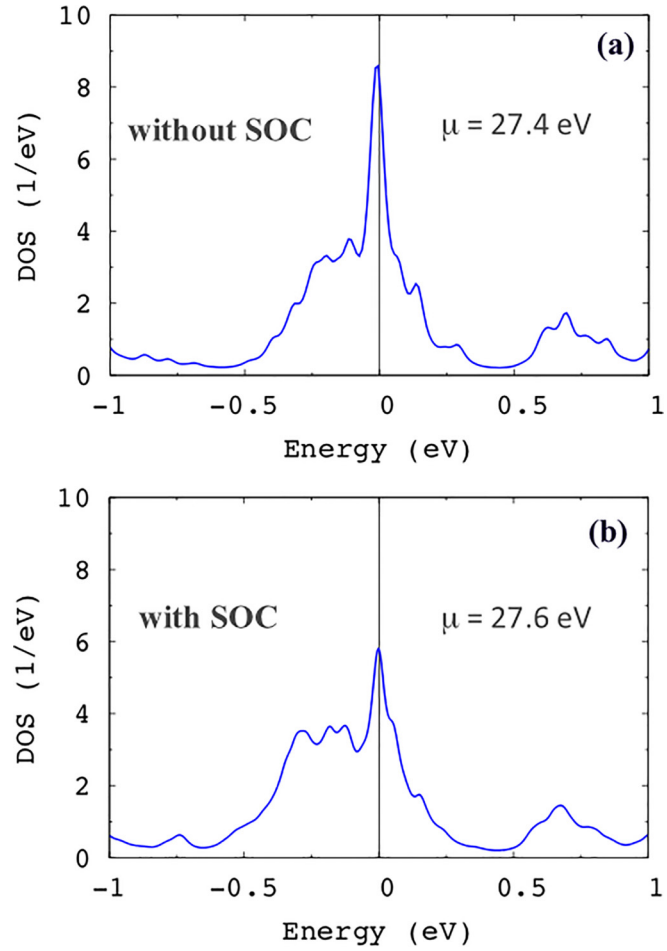

FIG. 3. (a) DOS for the Co@Cu(001) for $\mu = 27.4$ eV without SOC and (b) for $\mu = 27.6$ eV with SOC.

reduced while d^9, ^2D ($P_{d^9} \approx 0.3$) are increased. Again, there are no charge fluctuations near the GS. This GS looks similar to the $S = 1/2$ doublet (see Table III).

When the SOC is included, for values of $\mu = 26$ and 27 eV, the eigenstate $|\Omega\rangle_{N=26}$ is split into the lowest-energy singlet plus excited doublet (see Table III). These states approximately correspond to $|J = 1, J_z\rangle$ eigenstates of the effective Hamiltonian [30],

$$\hat{H}_{\mathrm{MA}} = D\hat{J}_z^2 + E\left(\hat{J}_x^2 - \hat{J}_y^2\right), \tag{4}$$

with the uniaxial magnetic anisotropy $D \approx 4.5$ meV, and $E = 0$. For $\mu = 28$ eV, the GS remains a $|\Omega\rangle_{N=27}$ doublet.

The corresponding densities of d states (DOS) for the values of $\mu = 26, 27$, and 28 eV are shown in Fig. 5, Appendix B. There are similarities in the DOS with and without SOC: no peak in DOS in a close vicinity of E_F. For these values of μ and without SOC there are no singlet GSs, and no Kondo resonances in the DOS. In the presence of SOC, even their GSs become singlets for $\mu = 26$ and 27 eV, and no Kondo peaks are formed. For $\mu = 28$ eV the GS solution remains a doublet without Kondo resonance in the DOS.

Since the change in the GS with a variation of μ between 27 and 28 eV is observed, we further adjust the values of μ in order to keep the same $n_d \approx 8$ without and with the SOC. In the case of $\mu = 27.4$ eV and without SOC, we obtain a non-integer $\langle N\rangle = 26.55$, nonzero $(\langle N^2\rangle - \langle N\rangle^2)^{\frac{1}{2}} \approx 0.5$ charge fluctuations, and $n_d = 7.93$. This solution is formally close to the "d^8" state but is actually a combination of d^7 ($P_{d^7} \approx 0.21$), d^8 ($P_{d^8} \approx 0.58$), and d^9 ($P_{d^9} \approx 0.18$) atomic states (see Table II).

There is a peak near E_F in the DOS shown in Fig. 3(a). Note that a similar peak in DOS was obtained in CTQMC calculations [10] without SOC with the same choice of Coulomb U and exchange J, and $n_d = 8$ very close to our calculations. In Ref. [10] it is interpreted as a spectral signature of the Kondo effect. As follows from Eq. (3), the presence of such a peak signals the (quasi)degeneracy of the eigenvalues E_N, and $E_{N\pm1}$. These are the $|\Omega\rangle_{N=27}$ doublet and $|\Omega\rangle_{N=26}$ triplet states which differ in energy by 1.2 meV (see Table III), with the doublet GS $|\Omega\rangle_{N=27}$. Since there is no singlet GS, the DOS peak at E_F is not a Kondo resonance, and signals the presence of valence fluctuations [30]. Moreover, the doublet GS can be interpreted as a signature of an underscreened Kondo state [10,23].

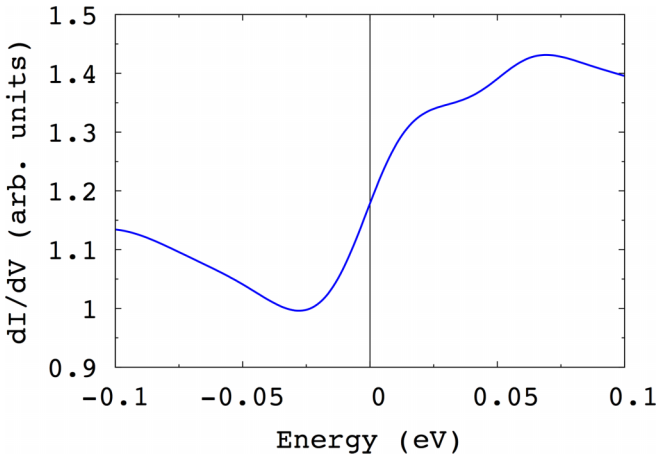

FIG. 4. Differential conductance $\mathcal{G}$ calculated making use of Eq. (6).

When the SOC is included, and with $\mu = 27.6$ eV, there is a noninteger $\langle N\rangle = 26.38$, with nonzero charge fluctuations $(\langle N^2\rangle - \langle N\rangle^2)^{\frac{1}{2}} \approx 0.5$, and $n_d = 7.96$ (see Table II). Again, the DOS has a peak at E_F which is shown in Fig. 3(b). In this case, the (quasi)degeneracy occurs between the singlet $|\Omega\rangle_{N=26}$ state being 1.9 meV lower in energy than the $|\Omega\rangle_{N=27}$ doublet (see Table III). The DOS peak at E_F due to the $|\Omega\rangle_{N=26}$-to-$|\Omega\rangle_{N=27}$ transition can be interpreted as a Kondo resonance.

For the singlet GS we can use the renormalized perturbation theory [13] in order to estimate the Kondo temperature,

$$T_K = -\frac{\pi}{4} Z \,\mathrm{Im}[\Delta(E_F)], \tag{5}$$

where an average quasiparticle weight per orbital Z is evaluated from

$$Z^{-1} \approx \frac{\mathrm{Tr}\{[\hat{I} - d\,\mathrm{Re}[\Sigma(\epsilon)]/d\epsilon(E_F)]A(E_F)\}}{\mathrm{Tr}[A(E_F)]},$$

following Ref. [31], and $A(E_F)$ is the DOS matrix from Eq. (3). We obtain $Z = 0.097$, and the corresponding $T_K = 0.019$ eV ($\approx$220 K). It exceeds the experimental estimate $T_K = 88$ K [3] of the Kondo scale. Indeed, Eq. (5) serves as an order of magnitude estimate of T_K.

Scanning tunneling spectroscopy measures the differential conductance $\mathcal{G}(V)$ through the adatom, and allows us to probe the DOS. A comparison between the experimental and theoretical $\mathcal{G}(V)$ is the most direct way to distinguish between different theoretical approximations and to identify the most appropriate theoretical approach. Experimentally $\mathcal{G}(V)$ of Co@Cu(100) was studied in Ref. [3]. The observed steplike behavior was interpreted in terms of interference between two tunneling channels: (i) tunneling to the d-DOS shown in Fig. 3, and (ii) tunneling into the conduction electrons of the Cu substrate modified by the presence of the Co adatom. At low bias, the differential conductance is then expressed [32] in the basis of cubic harmonics as

$$\mathcal{G}(\omega) \sim \sum_m (1 + \Gamma_m\{(1 - {q_m}^2)\,\mathrm{Im}[G_m(\omega)] + 2q_m\,\mathrm{Re}[G_m(\omega)]\}), \tag{6}$$

where $G_m(\equiv G_{mm})$ is a Green's function of the Hamiltonian Eq. (1), $\Gamma_m \equiv -\mathrm{Im}[\Delta_m(E_F)]$ is a hybridization between the d-level m and the substrate shown in Fig. 1(c), and q_m is a Fano parameter. For the strongly localized Co adatom d orbitals [33],

$$q_m \approx -\,\mathrm{Re}[G_{0,m}(E_F)]/\,\mathrm{Im}[G_{0,m}(E_F)].$$

The calculated $\mathcal{G}(V)$ is shown in Fig. 4 in fair quantitative agreement with the experimental data [3]. Note that our results seem to agree with the experiments better than those of Ref. [17]. Contrary to the proposal of Ref. [17], attempting to explain the zero-bias anomaly in Co@Cu(100) as the results of inelastic spin excitations, our theory demonstrates that they can be better explained from the point of view of the "Kondo" physics.

IV. SUMMARY

Many-body calculations within the multiorbital SIAM for an Co adatom on a Cu(100) surface are performed. DFT calculations were used to define the input for the discrete bath model of 40 bath orbitals, and with SOC included. We found that the peak in the DOS at E_F can occur for the Co atom d-shell occupation $n_d \approx 8$, and is connected to the quasidegenerate ground state of the SIAM. Without SOC, the lowest-energy state is an effective $S = 1/2$-like doublet, and next to it there is an effective $S = 1$-like triplet, so the resonance in the DOS(E_F) does not represent a Kondo resonance. When SOC is included, the triplet states are split as $|J = 1, J_z\rangle$ eigenstates in the presence of magnetic anisotropy $\hat{H}_{\mathrm{MA}} = D\hat{J}_z^2$, so that the $|J = 1, J_z = 0\rangle$ singlet becomes a ground state. The corresponding DOS(E_F) peak corresponds to Kondo resonance. This solution is verified by comparison with an experimentally observed zero-bias anomaly in the differential conductance. Our calculations illustrate the essential role which the SOC, and the corresponding uniaxial magnetic anisotropy, is playing in the formation of a Kondo singlet in multiorbital low-dimensional systems.

ACKNOWLEDGMENTS

Financial support was provided by Operational Programme Research, Development and Education financed by European Structural and Investment Funds and the Czech Ministry of Education, Youth and Sports (Project No. SOLID21 - CZ.02.1.01/0.0/0.0/16_019/0000760), and by the Czech Science Foundation (GACR) Grant No. 21-09766S. The work of A.I.L. is supported by European Research Council via Synergy Grant No. 854843 - FASTCORR.

APPENDIX A: FITTING THE BATH HYBRIDIZATION

With the specific choice of Cartesian reference frame (see Fig. 1), the local Green's function $G_0(z)$ becomes diagonal in the basis of cubic harmonics $m = \{xz, yz, xy, x^2 - y^2, 3z^2 - r^2\}$. Moreover, it is convenient to use an imaginary energy axis over the Matsubara frequencies $i\omega_n$. The corresponding

TABLE IV. Values of the d-shell $\Delta_{\rm CF}$ (eV), the bath energies ϵ_m^k (eV), and hybridization parameters V_m^k (eV) evaluated from LDA.

m	xz	yz	xy	x^2-y^2	$3z^2-r^2$
$\Delta_{\rm CF}$	−0.043	−0.043	0.117	0.053	−0.082
$\epsilon_{k=1,m}$	−2.16	−2.16	−1.99	−2.01	−2.57
$V_{k=1,m}$	0.85	0.85	0.65	0.65	0.72
$\epsilon_{k=2,m}$	−0.08	−0.08	0.001	−0.02	−0.05
$V_{k=2,m}$	0.18	0.18	0.08	0.10	0.13
$\epsilon_{k=3,m}$	0.51	0.51	1.45	0.53	0.43
$V_{k=3,m}$	0.36	0.36	0.55	0.34	0.32
$\epsilon_{k=4,m}$	7.56	7.56	7.80	8.16	7.72
$V_{k=4,m}$	2.08	2.08	2.12	1.78	1.70

noninteracting Green's function of Eq. (1) will then become

$$G_{0,m}(i\omega_n) = \frac{1}{i\omega_n - \epsilon_m - \Delta_m(i\omega)},$$

with the hybridization function

$$\Delta_m(i\omega_n) = i\omega_n - \epsilon_m - G^{-1}_{0,m}(i\omega_n). \tag{A1}$$

Thus, the hybridization function Eq. (A1) can be evaluated making use of the local Green's function $G_0(z)$. The discrete bath model is built by finding bath energies and amplitudes which reproduce the continuous hybridization function as closely as possible,

$$\tilde{\Delta}_m(i\omega_n) = \sum_{k=1}^{K} \frac{V_{km}^2}{i\omega_n - \epsilon_{km}}. \tag{A2}$$

The fitting is done by minimizing the residual function,

$$f_m(\{\epsilon_{km}, V_{km}\}) = \sum_{n=1}^{N_\omega} \frac{1}{\omega_n^\gamma} |\tilde{\Delta}_m(i\omega_n) - \Delta_m(i\omega_n)|^2, \tag{A3}$$

using the limited-memory, bounded Broyden-Fletcher-Goldfarb-Shanno method [34,35], with the parameters ϵ_{km} and V_{km} as variables. The factor $\frac{1}{\omega_n^\gamma}$ with $\gamma = 0.5$ is used to attenuate the significance of the higher frequencies. The fitted bath parameters are shown in Table IV. These parameters are used to build the AIM Hamiltonian Eq. (1).

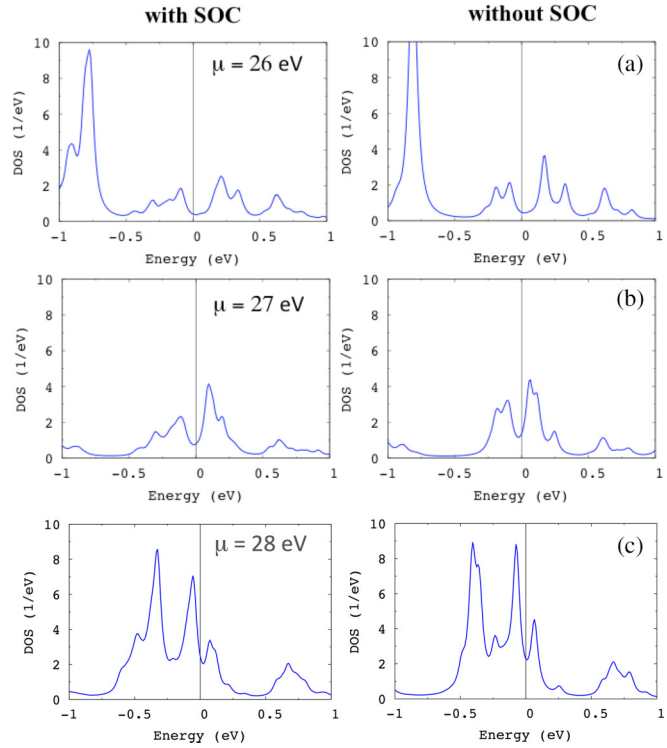

FIG. 5. DOS for the Co@Cu(001) with and without SOC as a function of (a) $\mu = 26$ eV, (b) 27 eV, and (c) 28 eV.

APPENDIX B: DOS AS A FUNCTION OF μ FOR CO ON CU(001)

The Co atom d-states projected DOS for the values of $\mu =$ 26 eV, 27 eV, 28 eV are shown in Fig. 5.

[1] G. D. Mahan, *Many-Particle Physics* (Springer, Boston, MA, 2000).
[2] P. Monod, Phys. Rev. Lett. **19**, 1113 (1967).
[3] N. Knorr, M. A. Schneider, L. Diekhöner, P. Wahl, and K. Kern, Phys. Rev. Lett. **88**, 096804 (2002).
[4] A. Zhao, Q. Li, L. Chen, H. Xiang, W. Wang, S. Pan, B. Wang, X. Xiao, J. Yang, J. Hou *et al.*, Science **309**, 1542 (2005).
[5] A. A. Abrikosov, Physics Physique Fizika **2**, 5 (1965).
[6] H. Suhl, Phys. Rev. **138**, A515 (1965).
[7] Y. Nagaoka, Phys. Rev. **138**, A1112 (1965).
[8] P. Wahl, L. Diekhöner, M. A. Schneider, L. Vitali, G. Wittich, and K. Kern, Phys. Rev. Lett. **93**, 176603 (2004).
[9] B. Surer, M. Troyer, P. Werner, T. O. Wehling, A. M. Läuchli, A. Wilhelm, and A. I. Lichtenstein, Phys. Rev. B **85**, 085114 (2012).
[10] A. Valli, M. P. Bahlke, A. Kowalski, M. Karolak, C. Herrmann, and G. Sangiovanni, Phys. Rev. Res. **2**, 033432 (2020).
[11] U. Fano, Phys. Rev. **124**, 1866 (1961).
[12] A. N. Rubtsov, V. V. Savkin and A. I. Lichtenstein, Phys. Rev. B **72**, 035122 (2005).
[13] A. C. Hewson, *The Kondo Problem to Heavy Fermions* (Cambridge University Press, Cambridge, UK, 1993).
[14] P. Hohenberg and W. Kohn, Phys. Rev. **136**, B864 (1964).
[15] N. Parragh, A. Toschi, K. Held, and G. Sangiovanni, Phys. Rev. B **86**, 155158 (2012).
[16] M. Wallerberger, A. Hausoel, P. Gunacker, A. Kowalski, N. Parragh, F. Goth, K. Held, and G. Sangiovanni, Comput. Phys. Commun. **235**, 388 (2019).
[17] J. Bouaziz, F. S. M. Guimarães, and S. Lounis, Nat. Commun. **11**, 6112 (2020).
[18] G. Kresse and J. Furthmüller, Comput. Mater. Sci. **6**, 15 (1996).
[19] A. Georges, G. Kotliar, W. Krauth, and M. J. Rozenberg, Rev. Mod. Phys. **68**, 13 (1996).

[20] A. I. Lichtenstein and M. I. Katsnelson, Phys. Rev. B **57**, 6884 (1998).
[21] E. Wimmer, H. Krakauer, M. Weinert, and A. J. Freeman, Phys. Rev. B **24**, 864 (1981).
[22] W. Mannstadt and A. J. Freeman, Phys. Rev. B **55**, 13298 (1997).
[23] D. Jacob, J. Phys.: Condens. Matter **27**, 245606 (2015).
[24] A. MacDonald, W. Pickett, and D. Koelling, J. Phys. C: Solid State Phys. **13**, 2675 (1980).
[25] V. I. Anisimov, J. Zaanen, and O. K. Andersen, Phys. Rev. B **44**, 943 (1991).
[26] I. V. Solovyev, P. H. Dederichs, and V. I. Anisimov, Phys. Rev. B **50**, 16861 (1994).
[27] M. Tchaplianka, A. B. Shick, and J. Kolorenc, J. Phys.: Conf. Ser. **2164**, 012045 (2022).
[28] K. Yosida, Phys. Rev. **147**, 223 (1966).
[29] G. Bergmann, Phys. Rev. Lett. **57**, 1460 (1986).
[30] M. Tchaplianka, A. B. Shick, and A. I. Lichtenstein, New J. Phys. **23**, 103037 (2021).
[31] L. V. Pourovskii, G. Kotliar, M. I. Katsnelson, and A. I. Lichtenstein, Phys. Rev. B **75**, 235107 (2007).
[32] K. R. Patton, S. Kettemann, A. Zhuravlev, and A. Lichtenstein, Phys. Rev. B **76**, 100408(R) (2007).
[33] T. O. Wehling, H. P. Dahal, A. I. Lichtenstein, M. I. Katsnelson, H. C. Manoharan, and A. V. Balatsky, Phys. Rev. B **81**, 085413 (2010).
[34] C. Zhu, R. H. Byrd, P. Lu, and J. Nocedal, ACM Trans. Math. Software **23**, 550 (1997).
[35] J. L. Morales and J. Nocedal, ACM Trans. Math. Software **38**, 1 (2011).